6

Corrosion Resistant Coatings Based on Organic-Inorganic Hybrids Reinforced by Carbon Nanotubes

Peter Hammer, Fábio C. dos Santos,
Bianca M. Cerrutti, Sandra H. Pulcinelli and Celso V. Santilli
Instituto de Química, UNESP-Univ Estadual Paulista, Brazil

1. Introduction

Composite materials can be prepared by the combination of at least two different phases, a continuous and a dispersed one. If one of these phases is on the nanometer scale, than the material is called a nanocomposite. In this context organic-inorganic hybrids stand for a new class of materials formed by two distinct compounds, the polymeric and ceramic, resulting in a crosslinked amorphous nanocomposit exhibiting different properties than the initial phases. The appropriate choice of the type and proportion of ceramic and polymeric precursor results in unique properties of the hybrid material combining processability and flexibility of polymer compounds with thermal, chemical and mechanical stability of ceramic materials. (Zheludkevich et al., 2005; Wang & Bierwagen, 2009). This allows to design specific characteristics of the material for a wide range of applications. Different forms of organic-inorganic hybrids have been intensively studied due to their interesting mechanical, optical and thermal properties (Zheludkevich et al., 2005), resulting in a number of applications such as drug delivery systems, sensors, electrical and optical devices, catalysts and protective coatings (Landry et al., 1992; Sarmento et al., 2010). Due to their inert and nontoxic nature, hybrid coatings are considered among the existing corrosion inhibitors as the most promising candidates for environmentally compliant surface protection.

The preparation of organic-inorganic hybrid nanocomposits can be performed by different chemical and physical routes, resulting in a material in which the organic and inorganic phases interact by weak intermolecular forces (class I hybrid) or by establishment of covalent bonds (class II hybrid), forming in the latter case a dense cross-linked network (Zheludkewich et al., 2005). The most widely used method for the synthesis of hybrid materials is the sol-gel process, which does not require high temperatures or other extreme conditions, and provides homogenous, transparent and high purity material at low costs. The chemistry of the sol-gel process is based on the hydrolysis and polycondensation reactions of metal and semimetal alkoxides combined with the radical polymerization of the monomer of the organic precursor (Binkler & Scherer, 1990). To promote covalent bonds between the inorganic network and the organic compound often a coupling agent is used in

the form of alkoxide groups modified by a vinyl binder. Inorganic materials prepared by the sol-gel route such as SiO_2, Al_2O_3, ZrO_2, etc., have relatively high hardness and thermal stability, but they posses also a high porosity (Vasconcelos at al., 2000; Nazeri at al. 1997; Maslski at al., 1999). Thus the inclusion of an organic component in the pores of the inorganic phase produces an ultra-light, dense, flexible and resistant material with low internal stress, suitable for a number of applications (Sanches & Lebeau, 2004). Among the various available organic substituted trialkoxysilanes, (3-methacryloxy propyltrimethoxysilane (MPTS) has been successfully used as coupling agent between silica and poly(methyl methacrylate) (PMMA) phases prepared from the co-reaction of methyl methacrylate (MMA), tetra-alkoxysilanes such as tetraethyl orthosilicate (TEOS), and tetramethyl orthosilicate (TMOS) (Innocenzi at al., 2003; Herreld at al., 2003; Sarmento et al., 2006; Han et al., 2007). It is evident that the properties of hybrid materials are not just the sum of individual contributions of its constituents, there is a synergism that depends also on the chemical nature of organic-inorganic interface and the size and morphology of the involved phases (José & Prado, 2005).

Metallic corrosion is induced by the chemical reactions between the metal surface and the environment, leading to an irreversible disintegration of the material under formation of oxides, hydroxides and salts. In the case of steel and aluminum, Cl^-, O_2, and H_2O species, in addition to electron transport, play important roles in the corrosion process (Ryan at al., 2002; Betova et al., 2002). The corrosion resistance is strongly weakened when metallic materials are subjected to a medium containing chloride or moisture environment, with a tendency to suffer localized corrosion. This may result result in the loss of aesthetic appearance and structural integrity, and can be accompanied by the release of potentially toxic ions, which can be hindered by protective coating (Tsutsumi at al., 2007; Bhattacharyya et al., 2008; Lopez at al., 2008; De Graeve at al., 2007). The most common corrosion prevention method is the hexavalent chromium-conversion, which forms insoluble trivalent chromium products by metal dissolution followed by precipitation of a passive layer of corrosion product. This passive layer on aluminum and steel surfaces should be capable of resisting the chemical attack, thus preventing further metal oxidation. However due to the carcinogenic effects of hexavalent chromium-containing species, environmental regulations have mandated the near term removal of Cr(VI)-containing compounds from corrosion inhibiting packages.

In this context, the design of new materials that act as a barrier against the diffusion of aggressive species have been widely investigated, primarily driven by the need to replace the corrosion inhibitors based on chromates. For this purpose, different types of coatings have been developed, both organic (paints), and inorganic (ceramic or conversion such as anodization) as well as a combination of organic and inorganic compounds. However, films based on polymeric materials have low thermal stability and poor adhesion to metal surfaces, while inorganic coatings suffer limitations due to micro cracks, porosity and high internal stress leading to adhesion problems and thickness limitations. Alternatively, the research on organic-inorganic hybrid materials deposited by dip or spin-coating on various substrates, mostly metals, has intensified in recent years due to their excellent anti-corrosion performance (Sarmento et al., 2010; Kim et al., 2009). A variety of different compositions including siloxane-methacrylate and ZrO_2-PMMA hybrid systems have been studied

showing pronounced improvement of corrosion resistance of stainless steel alloys against corrosion under acidic conditions and in the presence of high concentrations of Cl^- ions (Messaddeq et al., 1999; Meteroke et al., 2002; Zandri-Zand et al. 2005; Zheng & Li, 2010). This is a consequence of their highly interconnected structure of ramified siloxane cross-link nodes interconnected by short polymeric chains forming a chemically inert barrier, which prevents the penetration of species that initiate corrosive processes (Sarmento et al., 2010). Detailed analysis of the system have shown that inorganic phase has an important role in promoting the adhesion between the film and metal substrate, while the organic phase hermetically seals the film structure (Sarmento at al., 2010). In addition, hybrid films exhibit hydrophobic character and as a consequence of their low intrinsic stress they can be prepared crack-free even with a thickness of several micrometers (Messaddeq et al., 1999; Sarmento at al., 2010). Several other aspects favor the use of these materials, among which can be highlighted the mild conditions of the sol-gel synthesis, the low costs of preparation, environmental compatibility and also the low temperatures needed to cure the coatings. Consequently, organic-inorganic hybrid films prepared via sol-gel process posses a great potential for large-scale application as protective coatings of metallic surfaces.

Recently, several studies reported on the improvement of the passivation character of hybrid coatings by the addition of species that act as corrosion inhibitors. In particular cerium III and IV ions has been shown to satisfy several basic requirements expected from a corrosion inhibitor, for example, to increase the degree of polycondensation of the amorphous network, to form insoluble nontoxic oxides and hydroxides, besides to be relatively cheap and easy to handle (Pepe et al., 2004). The effects of cerium ions in the structure of the hybrids deposited by dip-coating has been investigated by several authors (Pepe et al., 2004; Suegama et al., 2009), including our group (Hammer at al., 2010), showing from the analysis of nuclear magnetic resonance and X-ray photoelectron spectroscopy data the active role of Ce(IV) on the densification of the polysiloxane films, i.e., the finding that free radical reactions between neighboring silanol and ethanol groups, induced by the reduction of Ce(IV), increases the connectivity of the hybrid network, resulting in elevated corrosion protection efficiency of the coatings.

Another important issue is the thermal and mechanical stability of hybrid films. Composite materials like polymer and hybrid systems containing carbon nanotubes (CNTs) are gaining increasing space as a promising class of advanced materials (Kim at al., 2009). The high thermal and mechanical stability and chemical inertness of carbon nanotubes (Khare at al., 2005) makes them a very interesting candidate for the improvement the properties of horganic-inorganic hybrid materials. Recently, the incorporation of carbon nanotubes in polymers and hybrids has shown excellent results in terms of improvement of their mechanical stability (Eder, 2010; Kim at al., 2009). The inclusion of only 0.1 to 1.0 at.% of functionalized (Voiry at al., 2011) or doped (Droppa Jr., 2001) carbon nanotubes is sufficient to improve considerably the mechanical properties and to increases the electrical and thermal conductivity of nanocomposites (Eder, 2010). Applications of these highly resistant and lightweight materials are in fields of electronics, energy, chemical industry and construction including, among others, flexible polymers, epoxy resins, refractory materials and nanostructured concrete. Despite the increasing interest to reinforce different classes of materials by carbon nanotubes, the area of hybrid materials is still not much explored. To

improve the mechanical properties of organic-inorganic, carbon nanotubes functionalized by hydroxyl, amide or sulphate groups are of particular interest since they are able to promote covalent bonds with siloxane groups of the network. Thus from the conjugation of CNTs with organic-inorganic hybrid it is expected to obtain nanocomposite coatings that combine high anti-corrosion efficiency with elevated mechanical resistance. In addition, the metallic conduction of multi-wall nanotubes (MWCNTs) allows an increase in conductivity of the hybrids by several orders of magnitude. This effect in combination with an organic phase based on conjugated polymers (Sanches & Lebeau, 2004) can be exploited for the development of transparent conductive hybrid coatings with optimized passivating character, a material with the potential for numerous applications.

Considering the great potential and versatility of this new class of composite materials this work focuses on the investigation of sol-gel siloxane-polymethyl methacrylate hybrids conjugated with functionalized carbon nanotubes used as corrosion resistant coatings on carbon steel. Based on the correlation of structural data, obtained for hybrids containing different amounts of the organic phase, with their corrosion protection efficiency, the aim of this work was to identify the most suitable matrix for the incorporation of functionalized carbon nanotubes to reinforce the hybrid structure without degrading the corrosion protection character of the coatings. The structural features of the siloxane-PMMA hybrids were studied as a function of the PMMA fraction and carbon nanotubes concentration and ^{29}Si nuclear magnetic resonance (NMR), X-ray photoelectron spectroscopy (XPS) and thermogravimetric analysis (TGA) while the corrosion protection efficiency was investigated by electrochemical impedance spectroscopy (EIS) and potentiodynamic polarization curves, after immersion of the samples in a acidic and neutral saline solution.

The low carbon alloy steel was chosen as substrate since it combines properties such as high hardness, high toughness and high flexibility, besides being relatively inexpensive, easy to manufacture and having many functional applications such as automotive sheet metal, structural shapes, plates for production pipes, construction material, tin cans etc. However, corrosion is still a great obstacle when it comes to its durability, suffering severe corrosion when in contact with even low amounts of chloride ions and acid solutions.

2. Experimental procedure

2.1 Materials

The following reagents were used as received and are available commercially: tetraethylorthosilicate (TEOS, Aldrich), 3-methacryloxy propyltrimethoxy-silane (MPTS, Fluka), methyl methacrylate (MMA, Fluka), ethanol (Mallinckrodt) and tetrahydrofuran (THF, Mallinckrodt). The MMA was pre-distilled to remove the polymerization inhibitor (hydroquinone) and possible impurities. The benzoyl peroxide (BPO, Reagan) was recrystallized in ethanol solution. For doping experiments multi wall carbon nanotubes (Nanocyl) were used.

2.2 Preparation of the hybrids

The siloxane-polymethyl methacrylate hybrids were prepared using the sol-gel route in three stages: In the first step the monomer (MMA) and the alkoxide modified with a

methacrylate group (MPTS) were polymerized in THF using the thermal initiator (BPO). The reaction was carried out during 2 hours at temperature of 70 °C under constant stirring in a reflux flask. In the second step, the inorganic component of the hybrid was prepared by hydrolysis and condensation of silicon alkoxide (TEOS). The hydrolysis of TEOS was carried in an ethanol solution by addition of acidified water (pH 1) using nitric acid. After 1 h of reaction at 25 °C under constant stirring in a closed flask, in a final step, the inorganic component was added into the reflux flask containing the organic solution. At this stage the modified MPTS is partially hydrolyzed and condensed with the TEOS, forming a homogeneous and transparent sol used for the deposition of the films by dip-coating. The following thermal cure 150 °C ensured a high degree of polycondensation of the hybrid structure. To study the influence of the proportion of the organic component on the film structure and electrochemical properties, the hybrids were prepared with the following MMA to MPTS molar ratios: 2, 4, 6, 8 and 10, referred to as M2, M4, M6, M8 and M10, respectively. The other optimized molar ratios were kept constant: H_2O/Si = 3.5, etanol/H_2O = 0.5, BPO/MMA = 0.01 and TEOS/MPTS = 2.0 (Sarmento et al., 2010).

2.3 Preparation of hybrids modified by carbon nanotubes

One of the hybrid samples with a higher fraction of silica and good anti-corrosion performance (M4) was chosen for the incorporation of functionalized carbon nanotubes (CNTs). The CNTs were functionalized by carboxyl groups in a standard oxidation procedure using a mixture of sulfuric and nitric acid (3:1) under reflux during 4 h at 70 °C. After dispersion in 0,5 L of deionized water and a short ultrasonic treatment the CNTs were filtered and annealed during 12 h at 200 °C. Finally, the functionalized carbon nanotubes were dispersed in a solution of ethanol containing Nafion® 5% and then added to the inorganic component of the hybrid. To study the influence of the CNTs content on film structure and electrochemical properties of the M4 sample, the following $[C_{CNT}]/[C_{CNT}+ Si]$ atomic concentrations were used: 0.1%, 1.0% and 5.0%, referred to as M4_01, M4_1 and M4_5, respectively. The aspect of the samples M4 and M4_5 obtained after 5 days of gelatinization are shown in Figure 1. Although the sample containing CNTs showed a dark coloration, the films deposited on steel hat the same colorless and transparent aspect as the undoped coatings.

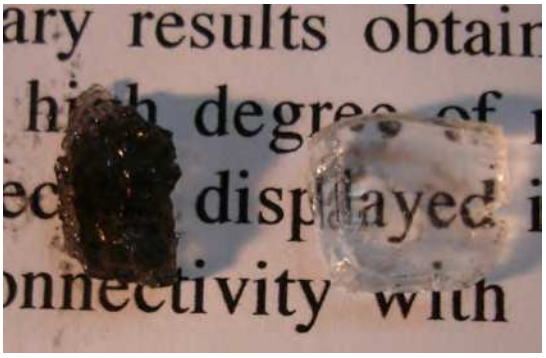

Fig. 1. Hybrid gel samples prepared at MMA/MPTS ratio of 4, M4 without CNTs (transparent) and M4_5, containing CNTs (dark), obtained after 5 days of drying at 10 °C (see text for details).

2.4 Preparation of the substrates and film deposition

For electrochemical corrosion tests and XPS measurements, coated A1010 carbon steel substrates (25 mm x 20 mm x 5 mm) were used, having a nominal composition (wt%) of C = 0.08 to 0.13%, Mn = 0.3 to 0.6%, P = 0.04% max and S max = 0.05%, with the balance consisting of Fe. The deposition of hybrid films was performed by dip-coating process using a dip-coater (Microchemistry - MQCTL2000MP), optimized at a rate of 14 cm min^{-1}, with 1 min of immersion and air-drying during 10 min at room temperature. This procedure was performed three times for each sample. Then the coated substrates were heated at 60 °C for 24 h. Finally, the samples were subjected to further heat treatment at 160 °C during 3 h. The thermal treatment at 60 °C favors the radical polymerization (initiated by BPO) of methacrylate groups of MPTS and of MMA monomers in the film and the cure at 160 °C was carried out to ensure the entire removal of all solvents, to complete the polymerization process of organic compounds and to densify the film. Homogeneous, transparent, crack-free coatings were produced. The coating thickness was determined by profilometry (Talystep, Taylor & Hobson). The adhesion of the films to the steel surface was carried out using a PosiTest Pull-Off Adhesion Tester (De Felsko), testing the coating´s strength of adhesion to the substrate by determining the tensile pull-off force of detaching.

2.5 Characterization methods

Unsupported hybrid films for NMR and TGA analysis were obtained by drying the sols in a Petri dish at 60 °C for 24 h. After the curing process, at 160 °C for 3 h, the films were detached from the dish and milled to obtain a powder. To obtain structural information solid-state ^{29}Si magic-angle spinning nuclear magnetic resonance (MAS-NMR) spectra were recorded for powder samples using a VARIAN spectrometer operating at 300 MHz and 7.05 T. The Larmor frequency for ^{29}Si was 59.59 Hz. The spectra were obtained from the Fourier transformation of the free induction decays (FID), following a single $\pi/2$ excitation pulse and a dead time of 2 s. Chemical shifts were referenced to tetramethylsilane (TMS), used as external standard. Proton decoupling was always used during spectra acquisition. Because of the high sensitivity of the ^{29}Si NMR measurements, the uncertainty in the chemical shift values was less than 0.2 ppm.

The TGA curves of powder samples were recorded using a SDT Q600 (TA Instruments) thermal analysis system, with nitrogen as purge gas at a flow rate of 70 ml min^{-1}. About 7 mg samples of hybrids were placed into platinum crucibles, and heated at a rate of 10 °C min^{-1} up to 600 °C.

The XPS analysis was carried out at a pressure of less than 10^{-6} Pa using a commercial spectrometer (UNI-SPECS UHV) to verify the changes in of the local bonding structure of samples containing different amounts of polymeric phase and carbon nanotubes. The Mg Kα line was used (hν= 1253.6 eV) and the analyzer pass energy for the high-resolution spectra was set to 10 eV. The inelastic background of the C 1s, O 1s and Si 2p electron core-level spectra was subtracted using Shirley's method. Due to charging of the samples, the binding energies of the spectra were corrected using the hydrocarbon component of adventitious carbon fixed at 285.0 eV. The composition of the near surface region was determined with an accuracy of ±10% from the ratio of the relative peak areas corrected by Scofield's sensitivity factors of the corresponding elements. The spectra were fitted without

placing constraints using multiple Voigt profiles. The width at half maximum (FWHM) varied between 1.0 and 2.0 eV and the accuracy of the peak positions was ±0.1 eV.

The polarization resistance of coated and uncoated steel samples was evaluated by means of electrochemical measurements carried out at 25 °C in 400 mL of naturally aerated and unstirred 0.05 mol L^{-1} H_2SO_4 + 0.05 mol L^{-1} NaCl solution and in neutral 3.5% NaCl solution. An $Ag/AgCl/KCl_{sat}$ electrode, connected to the working solution through a Luggin capillary, was used as reference, and a Pt grid as the auxiliary electrode. The working electrode was mounted in an EG&G electrochemical flat cell, exposing a geometric area of 1 cm^2 to the solution. This area is generally different of the actual area exposed to the solution, since it depends on the electrolyte penetration, surface roughness and on the many defects present in the layer (Suegama et al., 2006).

Polarization curves were recorded for all samples using a potentiostat/galvanostat (EG&G Parc-273), over the potential range -150 mV to +1000 mV versus the open circuit potential, E_{OC}, referred to the $Ag/AgCl/KCl_{sat}$ electrode, at a scan rate of 0.167 mV s^{-1}. The polarization curves were recorded after 4 hours immersion in the electrolyte. The corrosion potentials and apparent corrosion current density values were directly estimated from classical *E* (mV) *vs. log i* (A cm^{-2}) curve. The Stern-Geary equation (Stern & Gaery, 2006) was not utilized, since not all conditions required for its use were fulfilled in the system studied. The Stern-Geary relationship can only be applied for general corroded surfaces when the conditions necessary to deduce the Buthler-Volmer equation are valid. This means that the polarization resistance should be equal to the charge transfer resistance of the corrosion reaction (Feliu et al., 1998). However, the polarization resistance can be comprised of diffusion resistance, adsorption resistance, ohmic resistance and other resistances, as a result of which the conditions needed for using the Stern-Geary equation are often not fulfilled. Therefore, discussion of the corrosion mechanism based on polarization curves was ruled out. For that reason, the polarization curves were qualitatively analyzed and only used to compare the coated materials with different formulation. To guarantee the reproducibility of the results all electrochemical measurements were performed in duplicate.

In another series of experiments, open circuit potential (EOC) and electrochemical impedance spectroscopy (EIS) measurements were performed for M2, M4, M8 and M10 samples after 1 day of immersion in acidic NaCl solutions. For the M8 sample, considered to be the hybrid coating with the best performance, the EIS studies were conducted for up to 18 days of immersion in saline solution. The EIS measurements were performed using a Potentiostat/Galvanostat EG&G Parc-273 and a Frequency Response Analyzer Solartron-SI1255 coupled to a computer. The EIS tests were performed applying 10 mV (rms) to the E_{OC} value, starting from 10^5 to $5x10^{-3}$ Hz with 10 points/decade. A 0.1 μF capacitor was connected to a platinum wire and a reference electrode to avoid phase shifting at high frequencies and noise at low frequencies. For all samples, E_{OC} was measured for 2 h, time enough to stabilize the potential value. Afterwards, the E_{OC} value was applied for 15 min with simultaneous measuring of the current, which stabilized during this time, and the impedance spectra were immediately recorded in 3.5% NaCl and in acidic chloride-containing solution. The experiments were performed in duplicate.

Finally, atomic force microscopy (AFM) measurements were carried out using the standard tapping mode of the Aglient 5500 instrument, the morphology of the surface as investigated

by field emission guns scanning electron microscopy (FEG-SEM) in the secondary electrons mode at 3 kV (JEOL 71500F) and the contact angle measurements were carried out by the sessile drop method using an OCA-20 Contact Angle System (DataPhysics Instruments).

3. Results and discussion

3.1 Pure hybrids

3.1.1 Structural analysis

AFM images of the hybrid coating showed a very smooth surface with an RMS roughness of less than 0.2 nm (M2). Inspections by optical microscopy and scanning electron microscopy (Fig. 2) confirmed that the transparent films are homogeneous and defect-free. The film thickness, determined by profilometry, was about 1.5 μm for the M2 coating. The tensile pull-off force of detaching was for all coatings higher than the 8 MPa limit of the PosiTest Pull-Off Adhesion Tester.

Figure 3 shows ^{29}Si NMR spectra for unsupported siloxane-polymethyl methacrylate hybrids prepared with MMA/MPTS molar ratios of 2, 4, 8 and 10 (M2, M4, M8 and M10). The main spectral feature of the samples is the broad resonance with peaks at -59 and -65 ppm, assigned to T^2 ($-CH_2Si(OSi)_2(OR)$, R = H or CH_3) and T^3 ($-CH_2Si(OSi)_3$) units, which are related to the polycondensation product of MPTS (Saravanamuttu et al., 1998; Tadanaga et al., 2000). Resonances related to TEOS polycondensation products are observed, at approximately -92, -102 and -109 ppm, which correspond to Q^2 ($Si(OSi)2(OR)2$), Q^3 ($Si(OSi)_3(OR)$) and Q^4 ($Si(OSi)_4$) species, respectively (Fedrizzi at al., 2001; Saravanamuttu et al., 1998; Tadanaga et al., 2000). The absence of monomer species T^0 (-CH2Si(OR)3) and Q^0 ($Si(OR)_4$) is in agreement with the cluster-cluster condensation mechanism, which is expected under strongly acid conditions (Han at al., 2000). The proportions of T^J and Q^J species present in the hybrid nanocomposit were extracted from the spectra by a peak fitting procedure used to determine the relative peak area of each species. As expected, the intensity ratio of Q^J/T^J species was found to be approximately 2, in agreement with the proportions of the TEOS and MPTS precursors used in the sample synthesis, which differed only in the fraction of the organic phase. The degree of condensation ($\%C_d$) of the inorganic phase in the unsupported polysiloxane hybrid was calculated from the proportions of each T^J and Q^J species according to the following equation (Saravanamuttu et al. 1998):

$$\%C_d = [(T^1 + 2T^2 + 3T^3)/3 + (Q^1 + 2Q^2 + 3Q^3 + 4Q^4)/4] \times 100 \quad (1)$$

The degree of condensation obtained for M2, M4, M8 and M10 hybrids were 80.9±0.5%, 79.7±0.5%, 83.9±0.5% and 75.8±0.5%, respectively. This result shows that with exception of M10 all samples have a high and almost identical degree of condensation and thus a similar bonding structure of the inorganic phase. This is not surprising since all hybrids were prepared at a fixed TEOS/MPTS ratio, restricting the variability of the silica network. The slightly higher degree of condensation of M8 is due to the increase of both the T^3/T^2 and Q^4/Q^3 the ratio, suggesting that heterocondensation occurs between both the MPTS and TEOS and the TEOS hydrolyzed species. The pure connectivity of M10 is evident (increase of T^1 and Q^2), and probably related to the excess of polymeric phase hindering the cross-linking of silica. Similar connectivity values as observed for M8 were found for highly

corrosion resistant polysiloxane hybrids having equal TEOS/MPTS molar ratio, however without inclusion of the PMMA phase (Sarmento et al., 2010).

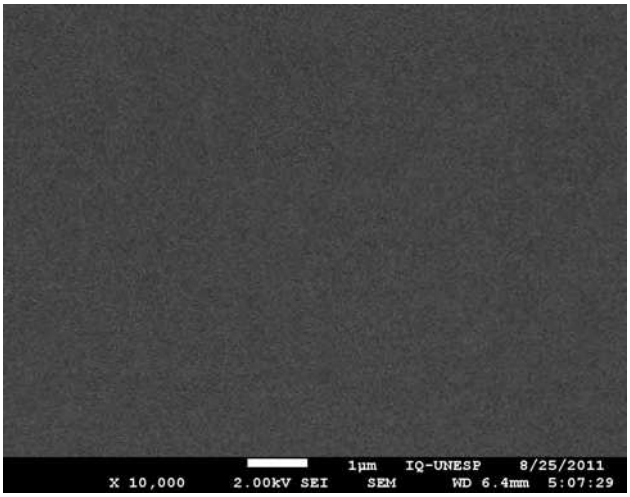

Fig. 2. Representative FEG-SEM image of the featureless surface of hybrid films (M4).

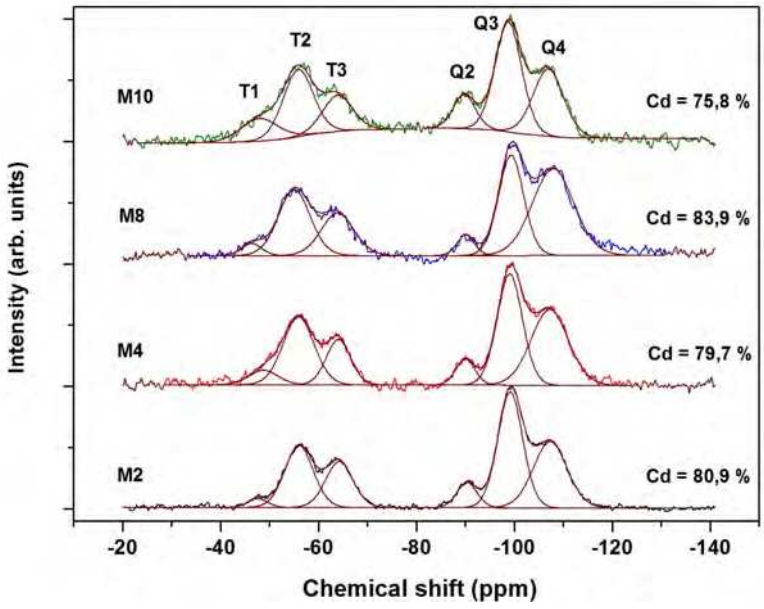

Fig. 3. ^{29}Si NMR spectra of hybrids prepared with MMA/MPTS ratios of 2 (M2), 4 (M4), 8 (M8) and 10 (M10).

The polymerization of the organic moieties was confirmed by the TGA curves and the differential weight loss (DTG) of unsupported siloxane-polymethyl methacrylate hybrids,

shown in Figure 4. Since the sample were cured at 160° C the small weight loss observed below 110 °C is attributed to the water vapor adsorption. The DTG curves indicate the existence of three degradation stages. The first two events at about 240 °C and 390 °C correspond to the radical depolymerization of the organic polymer segments of the hybrid. The event observed at about 240 °C might be ascribed to scissions of the chain initiated from the vinylidene end, and the one in the range of 390 °C – 410 °C to random scission within the polymer chain (Han at al., 2000). The weak degradation stage above 450 °C, can be attributed to the dehydration of silanol groups corresponding to Q^2 and Q^3 species present in the SiO_2 network (Han at al., 2000). With exception of the M2 hybrid, showing the highest thermal stability of about 410 °C, the temperature corresponding to each degradation step remains essentially invariant, suggesting that all other hybrids have a similar silica backbone which is not essentially affected by the increasing presence of the polymerization phase. It is interesting to note that the less stable step, involving the scissions of head-to-head linkages in the PMMA homopolymer, is absent in the case of the unsupported hybrid films. This is another indication that the prepared hybrids possess a much higher thermal stability than the PMMA homopolymer.

It is important to note that structural characteristics of thin film produced by dip-coating and the thick bulk film formed in Petri dish, used for NMR and TGA analysis, were found be equal by XPS analysis, thus guarantying a consistent interpretation of structural and electrochemical data.

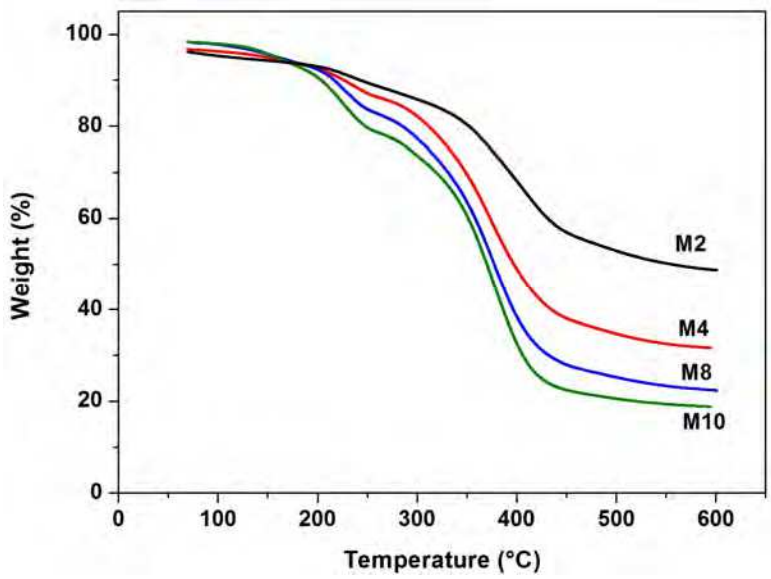

Fig. 4. TGA and DTG (insert) curves of hybrids prepared with MMA/MPTS ratios of 2 (M2), 4 (M4), 8 (M8) and 10 (M10).

X-ray photoelectron spectroscopy was used to obtain further information on the bonding structure and composition of the hybrid. The quantitative analysis showed that the detected

elemental concentrations is in agreement with the nominal composition of the samples, showing an increase of the atomic percentage of carbon from 51.9 at.% (M4) to 60.7 at.% (M10) accompanied by a reduction of oxygen content from 37.3.% (M4) to 33.1 at.% (M10) and of silicon from 10.8.% (M4) to 6.2 at.% (M10).

The structural evolution of the samples, with increasing TEOS/MPTS ratio, was evaluated from the fitted high-resolution C 1s, O 1s and Si 2p core level spectra, displayed in Figure 5.

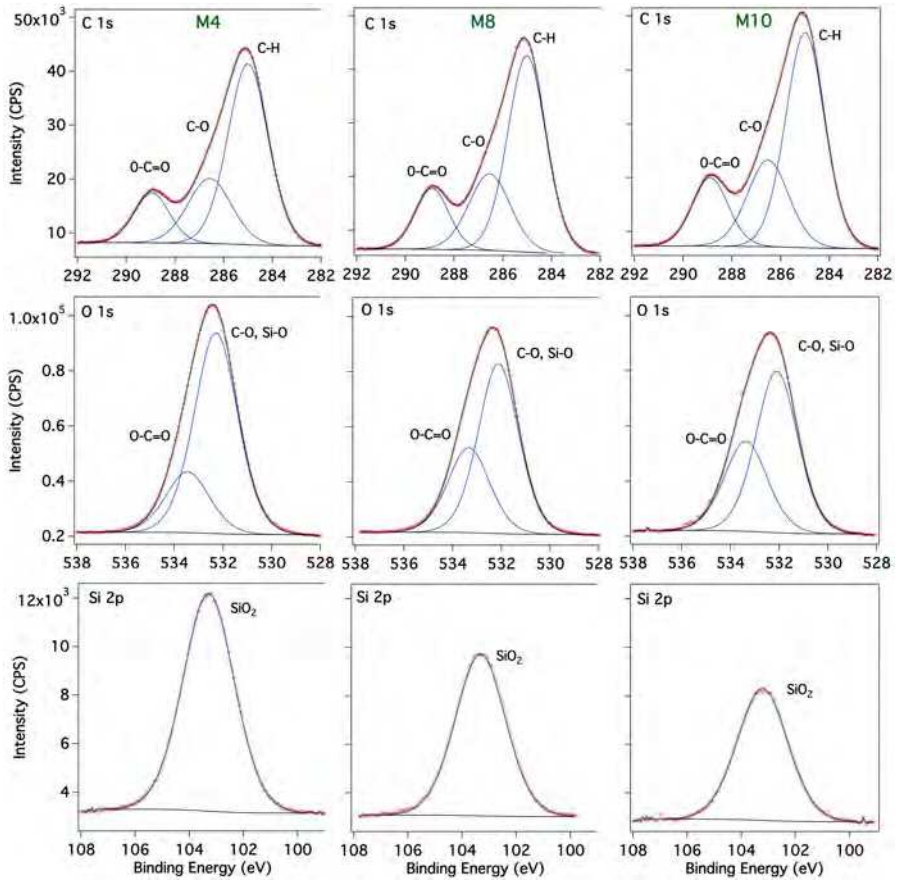

Fig. 5. Fitted XPS, C 1s, O 1s and Si 2p core level spectra of hybrids prepared with MMA/MPTS ratios of 4 (M4), 8 (M8) and 10 (M10).

The C 1s spectra show for all hybrids the presence of three different structural components of the organic phase, corresponding to hydrocarbon (C-H, at 285.0 eV), ether (C-O, at 286.6 eV) and ester (O-C=O, at 289.1 eV). It can be observed that with increasing fraction of the polymeric phase in the samples (M4, M8, M10) the intensity o the spectrum increases while intensity ratio of the sub-peaks I(C-H) : I(C-O) : I(O-C=O) remains constant, reflecting the preservation of the structural units of PMMA in the hybrid. The O 1s spectra were fitted with two components: the main peak located at 532.6 eV is related to C-O and Si-O bonds,

while the small component at about 534.0 eV can be assigned to a ester groups (already observed in the C 1s spectrum). The decrease of the intensity of the O 1s spectra and the increase of the ester component evidence the decreasing proportion of silica in the samples. Similar evolution was observed for the Si 2p spectra, showing the continuous decrease of its intensity upon increasing fraction of the polymeric phase.

3.1.2 Corrosion analysis

To investigate the corrosion protection performance of hybrids containing different fractions of polymeric phase electrochemical impedance spectroscopy curves were recorded after immersion periods of up to 3 days in acidic solution and up to 18 days in saline environment. Figure 6 displays the complex plane impedance and the Bode plots (log $|Z|$ and θ vs. log f) for the coated samples (M2, M4, M8, M10) and bare steel after exposure of 1 day in neutral saline solution and after a period of 3 days in acidic NaCl solutions. Compared to bare steel, the coated samples show up to 5 orders of magnitude higher impedance with best performance observed for the M8 hybrid coating, reaching about 1 GΩ in both environments. This value is about two orders of magnitude higher than the highest impedance reported for polysiloxane hybrids prepared with equal TEOS/MPTS molar ratio of 2 but without inclusion of MMA (Sarmento et al., 2010). The phase angle dependence shows a broad band extending from 5 mHz to 100 kHz, with θ values close to 90°, apparently with only one time constant close to 10 kHz. Tests with different equivalent circuits models have shown, however, a poorly defined time constant in the low frequency region. No significant change of the curve characteristics was observed after 3 days of exposure in acidic and 18 days in saline solution (Fig. 7), confirming the excellent performance of this coating. A similar high stability in both environments was observed for the M2 coating, having, however, two orders of magnitude lower corrosion resistance and a narrower θ frequency band. In contrast, for M4 and M10 coatings two well defined time constants were observed after 3 days of immersion in acid environment, with the low frequency time constant appearing at the position of the time constant of bare steel.

The electrical equivalent circuit used for fitting impedance experimental data for hybrid films in both environments is displayed in Figure 8. According to the standard interpretation used for coated metals, the time constant in the high frequency region (HF) is attributed to the hybrid coating properties (coating capacitance (CPE_1) in parallel with its resistance (R_1)), while that in the low frequency region (LF) is related to the properties of the oxidized steel at the film/steel interface (oxide capacitance (CPE_2) in parallel with its resistance (R_2)). The formation of this passive film is a result of the reaction with the solution, which penetrates the coatings after extended immersion periods. The obtained model parameters are displayed in Table 1 and Table 2 for samples immersed in neutral saline solution and acidic environment, respectively. Compared with the M8 coating a strong decrease of resistances R_1 and R_2 was observed for M2 and M4 in saline medium, while the capacitances remain essentially unchanged (Table 1, Fig. 5a). The long-term exposure of M8 confirmed the superiority of this coating, showing only a small reduction of R_1 after 18 days in saline environment (Table 1, Fig. 6). After 3 days of exposure in acid environment M8 maintained its inert character while the M4 coating showed signals of beginning degradation (Table 2, Fig. 5b). The appearance of the LF time constant and the

decrease of the capacitive character of the M4 and M10 coatings is indicative the beginning film failure after prolonged exposure in aggressive medium (Fig. 6c2). This is associated to electrolyte uptake, which increases the coating conductivity by the permeation of ionic species. For coatings M2 and M10 a corrosion process controlled by diffusion (Warburg element) cannot be excluded. Inspections by optical microscopy of these films revealed the formation of localized pits and the presence of iron species on the surface, detected by XPS.

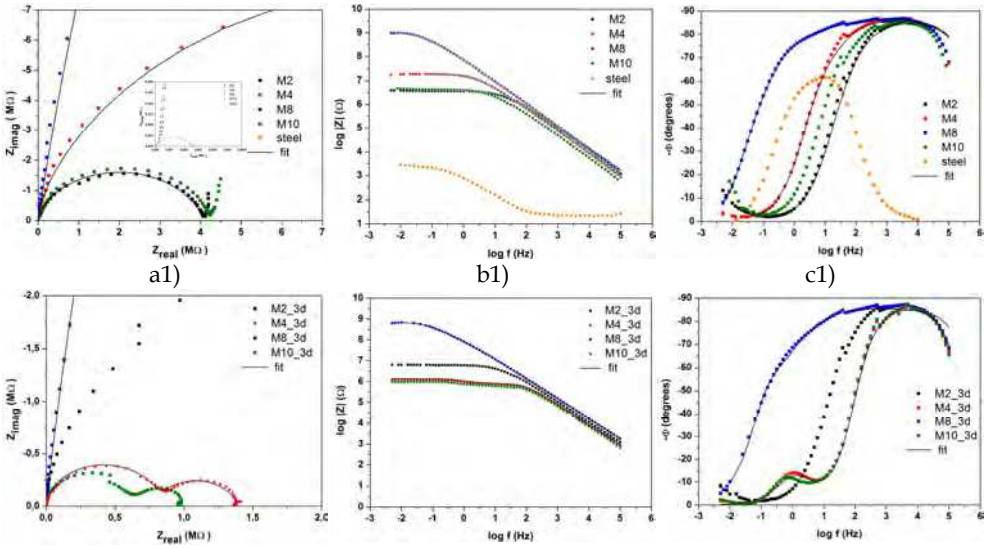

Fig. 6. Complex plane impedance (a), modulus impedance (b) and phase (c) plots of bare carbon steel and hybrids prepared with MMA/MPTS ratios of 2 (M2), 4 (M4), 8 (M8) and 10 (M10) after exposure of 1 day and 3 days in (1) unstirred and naturally aerated 3.5 % NaCl and (2) 0.05 mol L^{-1} NaCl + 0.05 mol L^{-1} H_2SO_4 solutions, respectively. (The small discontinuities of θ vs. log f mark the change of the measurement range of the instrument.)

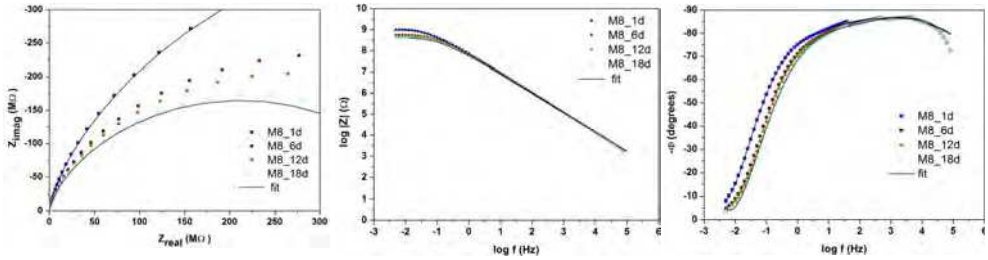

Fig. 7. Complex plane impedance (a), modulus impedance (b) and phase (c) plots of hybrids prepared with MMA/ MPTS ratios of 8 (M8) after exposure of up to 18 day in unstirred and naturally aerated 3.5% NaCl solution. (The small discontinuities of θ vs. log f mark the change of the measurement range of the instrument.)

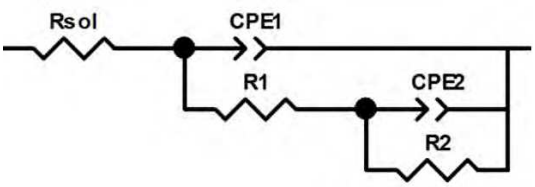

Fig. 8. Electrical equivalent circuit used for fitting impedance experimental data for hybrid films in 3.5 % NaCl and 0.05 mol L^{-1} H_2SO_4 + 0.05 mol L^{-1} NaCl solutions.

Sample	M8_1d	M8_18d	M4_1d	M2_1d
χ^2 (10^{-3})	9.8	6.4	9.7	9.5
R_{sol} (Ω cm^2)	22.7 (9.8)*	29.5 (4.4)	22.5 (7.8)	24.6 (7.8)
CPE_1 (10^{-3} μF cm^{-2} $s^{\alpha-1}$)	1.52 (28.9)	1.74 (4.2)	6.13 (16.3)	1.37 (16.9)
n_1	0.67 (7.6)	0.65 (4.5)	0.73 (8.1)	0.67 (7.4)
R_1 (10^6 Ω cm^2)	812 (12.5)	419 (2.9)	12.9 (11.6)	2.08 (16.5)
CPE_2 (10^{-3} μF cm^{-2} $s^{\alpha-1}$)	2.37 (3.4)	2.06 (2.4)	3.01 (3.1)	2.42 (4.9)
n_2	0.93 (6.4)	0.95 (0.25)	0.96(6.4)	0.95 (1.1)
R_2 (10^6 Ω cm^2)	305 (31.2)	26.9 (15.7)	6.72 (19.9)	2.01 (15.1)

*Error (%)

Table 1. Parameters of electrical equivalent circuit for sample M8, M4 and M2 after 1 day and 18 days (M8) immersion in neutral 3.5% NaCl aqueous solution.

Figure 9 displays the potentiodynamic polarization curves for uncoated, M2, M4, M8 and M10 coated carbon steel, recorded after 2 h of immersion in neutral NaCl solutions. As expected the polarization curve of the M8 coating, having the highest degree of condensation of the inorganic phase (highest degrees of condensation, see Fig. 3), exhibits the lowest current density of approximately 10^{-10} Acm^{-2}, a value about five orders of magnitude lower than that observed for bare steel. To our best knowledge such excellent anti-corrosion performance at similar experimental conditions was not yet reported in the literature for organic-inorganic hybrid films. The curve characteristics of M4 and M2 are quite similar, the latter showing slightly higher current densities. The negative open circuit potential of sample M10, found close to the value of bare steel, is most probably related to its less cross-linked network (see Fig. 3) suggesting a more open structure of this film. For all tested coatings no breakdown of the coating was observed in the positive potential branch even at overpotential of 1 V. The results obtained in acidic medium are very similar to those observed in the saline solution (not shown). According to the electrochemical results, the performance against corrosion can be established in the following order: M8 > M2 > M4 > M10 > steel. This result is in agreement with the sequence of increasing network connectivity values found by NMR.

Sample	M8_3d	M4_3d
χ^2 (10^{-3})	9.7	8.8
R_{sol} (Ω cm^2)	22.7 (9.8)*	29.4 (6.8)
CPE_1 (10^{-3} μF cm^{-2} s$^{\alpha-1}$)	1.56 (4.2)	0.04 (7.2)
n_1	0.65 (4.5)	0.86 (3.8)
R_1 (10^6 Ω cm^2)	754 (5.4)	0.56 (2.9)
CPE_2 (10^{-3} μF cm^{-2} s$^{\alpha-1}$)	1.52 (2.5)	2.60 (2.6)
n_2	0.95 (0.3)	0.97 (0.3)
R_2 (10^6 Ω cm^2)	49.1 (16.2)	0.83 (1.1)

*Error (%)

Table 2. Parameters of electrical equivalent circuit for sample M8 and M4 after 3 days immersion in 0.05 mol L^{-1} NaCl + 0.05 mol L^{-1} H_2SO_4 solution.

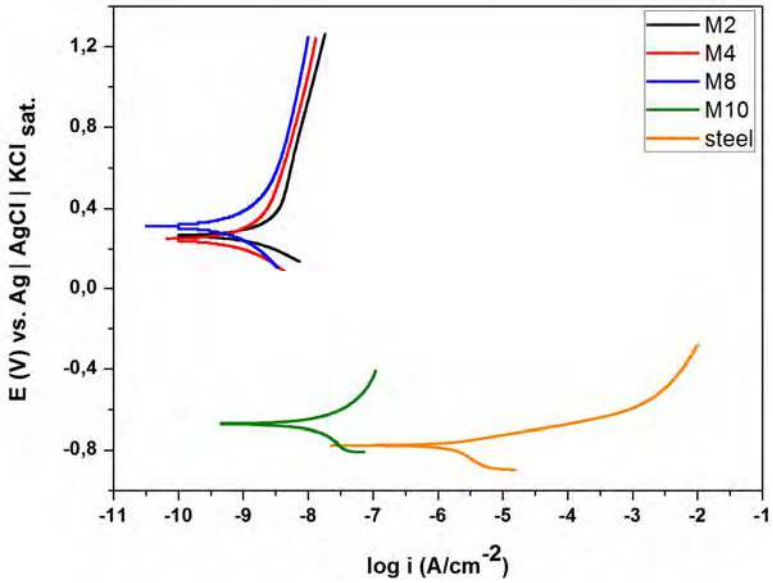

Fig. 9. Potentiodynamic polarization curves of bare carbon steel and hybrids prepared with MMA/MPTS ratios of 2 (M2), 4 (M4), 8 (M8) and 10 (M10) recorded after 2 h immersion in unstirred and naturally aerated 3.5 % NaCl solution.

3.2 Hybrids modified by carbon nanotubes

3.2.1 Structural analysis

For the experiments with samples containing functionalized carbon nanotubes the M4 hybrid was chosen due its higher fraction of silica and good anti-corrosion performance. Similar as in the case of pure hybrid films, AFM images of the M4_5 film, with a [C_{CNTs}]/[C_{CNT}+ Si] molar concentration of 5%, have shown a very smooth surface (R_{RMS} =

0.16 nm) without features which could be related to the presence of carbon nanotubes on the film surface (Fig. 10a), expected for MWCNTs at a scale of 10 – 20 nm. A featureless surface on the nanometer scale was also confirmed by FEG-SEM, as can be observed in Figure 10b. TThis indicates a very good dispersion of functionalized carbon nanotubes in the hybrid matrix. The film thickness, determined by profilometry, incrased from 1.5 μm to 2 μm with increasing CNTs content. The higher thickness detected for CNT rich samples is related to the increasing viscosity of the precursor solution. As already found for the CNT free samples the tensile pull-off force of detaching was for all coatings higher than 8 MPa. Furthermore, contact angle measurements have shown that no significant variation of the H_2O wetability (76±1° - 81±1°) of the film surface occurred with increasing CNTs content.

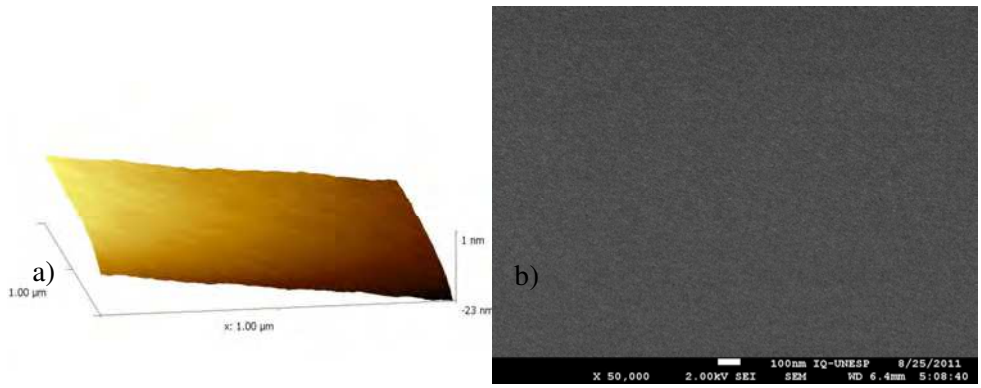

Fig. 10. Flat and featureless surface observed by a) AFM and b) FEG-SEM of the hybrid film prepared with a $[C_{CNT}]/[C_{CNT}+ Si]$ molar concentration of 5% (M4_5).

The verification of the degree of functionalization of the CNTs by carboxyl groups was performed using XPS. Figure 11 shows the C 1s core level spectra of as-received CNTs (Fig. 11a) and two functionalized samples after 4 h (Fig. 11b) and 8 h (Fig. 11c) of acidic treatment. The strong increase of the carboxyl component at about 288.8 eV evidences the increasing degree of functionalization with treatment time. From the intensity ratio of the O-C=O/C-C peak area a high functionalization degree of 0.15 and 0.35 was determined for the samples submitted to 4 h and 8 h of acid treatment, respectively. It cannot be excluded that, in the case of the latter sample, the high functionalization degree and the applied ultrasonic treatment of the precursor solution could lead to a significant fragmentation of the nanotubes (Voiry et al., 2011). Therefore, MWCNTs prepared after 4 h were used for the final formulation of the nanocomposit coating. Furthermore, it is important to point out that for the fitting of the aromatic carbon peak (C-C at 284.4 eV) an asymmetric Doniach-Sunjic function was used to account for the high density of states of multiwall carbon nanotubes at the Fermi level (Briggs & Seah, 1990). Thus it is possible to reduce the intensity of the carbon-oxygen bonds of the C 1s spectra in a way that the amount of these bonds is compatible with the oxygen concentration, determined from the integrated intensity of the O 1s peak.

Structural changes induced by the incorporation of increasing quantities of CNTs in the hybrid network were evaluated from the evolution of fitted XPS C 1s, O 1s and Si 2p core level spectra (Fig. 12). The samples were prepared with MMA/MPTS molar ratios of 4 (M4) containing carbon nanotubes with a $[C_{CNT}]/[C_{CNT}+ Si]$ molar concentration of 0.1% (M4_01) 1.0% (M4_1) and 5% (M4_5). The comparison of the C 1s spectral intensities (CPS) shows that the M4_1 and M4_5 sample contain a higher fraction of carboxyl groups than the M4 hybrid. The intensity of this sub-peak is comparable to that of the M10 sample, having a larger portion of these groups ester due to the higher content of the organic PMMA phase. This fact can be seen even clearer from the increase of the O-C=O component in the O 1s spectra. It is suggested that these additional carboxylic structures promote covalent bonds between the inorganic network and CNTs.

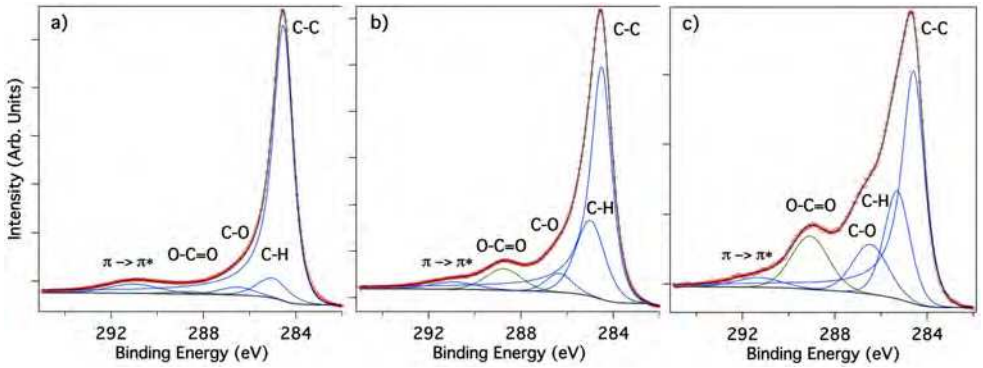

Fig. 11. Fitted XPS C1s core level spectra for a) as-received CNTs and b) after 2 h and c) 4 h of carboxyl functionalization by acidic treatment.

Figure 13 shows ^{29}Si NMR spectra for unsupported hybrid samples prepared at a MMA/MPTS ratio of 4 containing an increasing molar concentration of CNTs of 0% (M4), 0.1% (M4_01), 1.0% (M4_1) and 5% (M4_5). The degree of condensation extracted for the samples from the spectra were: 79.7±0.5%, 73.8±0.5%, 73.1±0.5% and 78.4±0.5%. Surprisingly, exactly for the sample containing the highest concentration of CNTs a similar degree of connectivity was found as for the M4 reference sample. Considering that the atomic concentration of silicon in the M4 hybrid, is close to 10 at.% (see XPS results), the carbon content related to CNTs of the sample M4_5 can be estimated to be about 0.5 at.%. This means that this considerable amount of CNTs is not affecting the high connectivity of the inorganic backbone structure of the M4 hybrid. In contrast, M_01 and M_1 hybrid show about 5% lower degrees of condensation, indicating the formation of a possibly less stable structure.

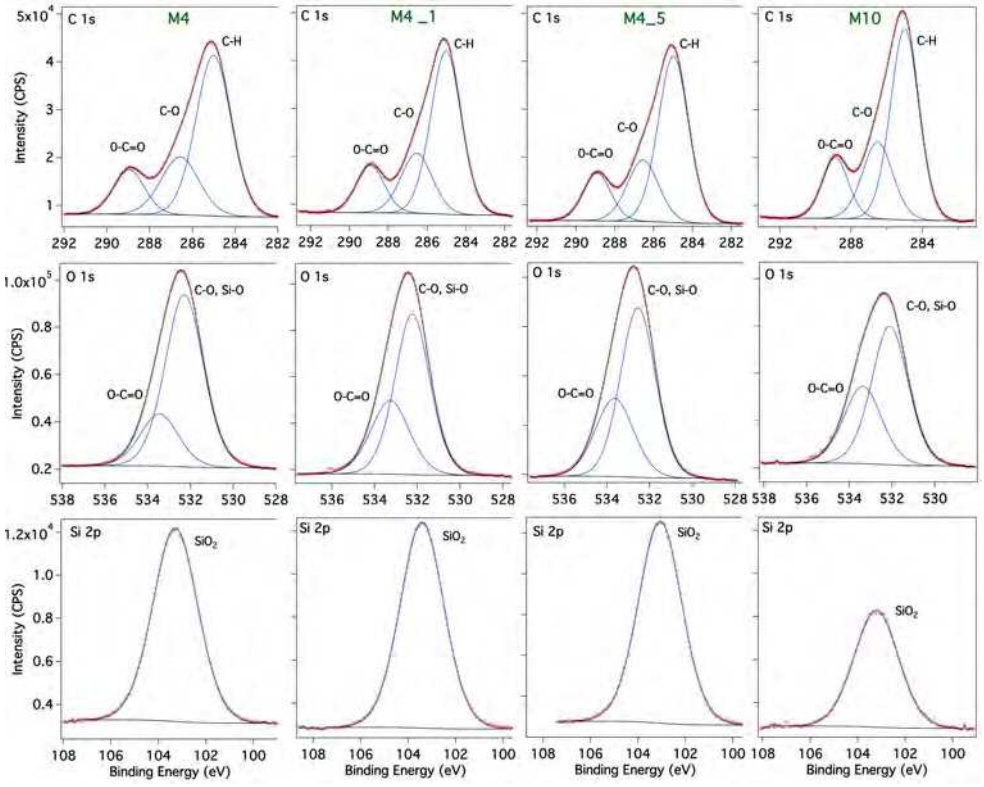

Fig. 12. Fitted XPS, C 1s, O 1s and Si 2p spectra of the hybrids prepared with MMA/MPTS ratios of 10 (M10) and 4 (M4) containing CNTs with $[C_{CNT}]/[C_{CNT}+ Si]$molar concentrations of 1.0% (M4_1) and 5% (M4_5).

The TGA and DTG curves of hybrids containing increasing amount of CNTs are shown in Figure 14. It is interesting to note, that in comparison to the M4 sample, the M4_5 hybrid displays two additional events at about 280 °C an 410 °C, the latter also observed for the M4_1 sample. The 410 °C event marks the thermal stability limit of these samples, a value found also for the M2 hybrid. As the intensity of the 280 °C event increases with the CNTs content, it is quite probable that this might be related to the liberation of functional groups, like carboxyls, attached to nanotube walls. From the TG/DTG results it can be concluded that the inclusion of higher quantities of CNTs maintains the thermal stability of the samples, indicating for these hybrids that the CNTs reinforce the structure possibly by the presence of covalent bonds with siloxane groups of the hybrid network.

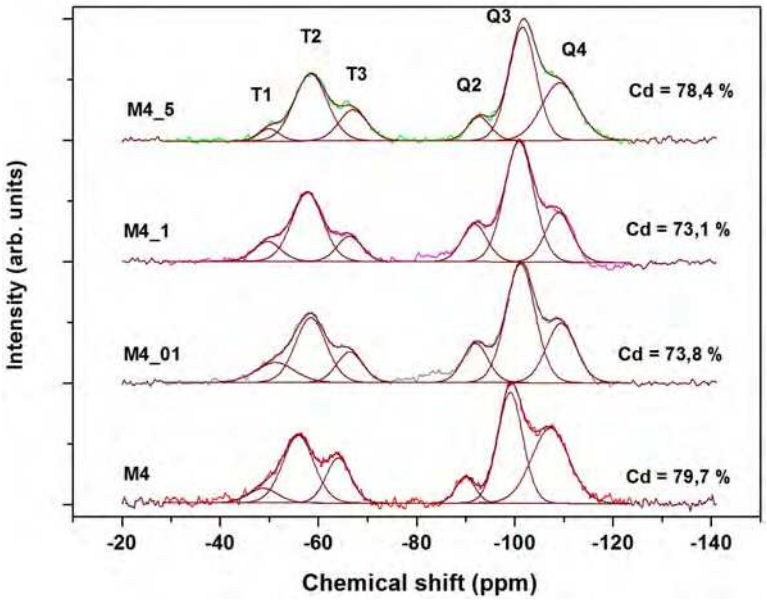

Fig. 13. ^{29}Si NMR spectra of hybrids prepared with a MMA/MPTS a ratio of 4 containing CNTs with $[C_{CNT}]/[C_{CNT}+ Si]$ molar concentrations of 0% (M4), 0.1% (M4_01), 1.0% (M4_1) and 5% (M4_5).

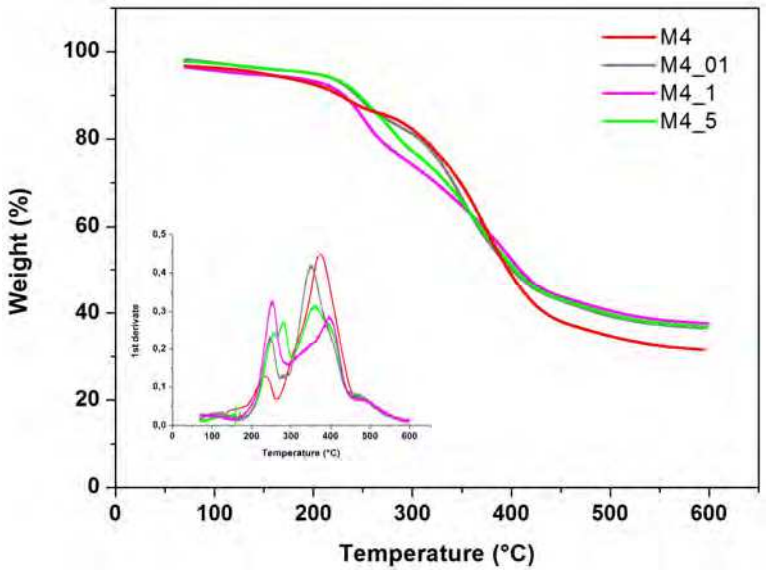

Fig. 14. TGA and DTG (insert) curves of hybrids prepared with a MMA/MPTS a ratio of 4 containing CNTs with $[C_{CNT}]/[C_{CNT}+ Si]$ molar concentrations of 0% (M4), 0.1% (M4_01), 1.0% (M4_1) and 5% (M4_5).

3.2.2 Corrosion analysis

The electrochemical characteristics of hybrids coatings containing different concentrations of carbon nanotubes was investigated using electrochemical impedance spectroscopy curves, recorded after 1 day of immersion in acidic and saline solution. Figure 15 shows the complex plane impedance and the Bode plots (log |Z| and θ vs. log f) for the M4 reference sample and the CNTs containing hybrid films M4_01, M4_1 and M4_5. Compared to the M4 film, the M_01 an M_5 films show a very similar characteristic in the saline solution. Only the M4_1 coating displays a second LF time constant, related to oxidized steel surface due to the penetration of the electrolyte to the film/steel interface. The beginning degradation can be associated with a less stable structure of this coating as suggested by the lowest degree of condensation, observed by NMR. The obtained model parameters are displayed in Table 3 show a slightly lower corrosion resistances of the M4_1 coating. A quite different behavior was observed after immersion of the samples into the acidic medium. While for the CNT coatings the corrosion resistance remains essentially unchanged a drop of the impedance, of more than one order of magnitude, was detected for the M4 coating. The inferior performance in acidic solution is also indicated by the appearance of the LF time constant, marking the initiation of film failure. This is also evidenced by the lower corrosion resistance of M4 compared to that of M4_5 sample (see Table 3). The obtained results suggest a superior performance of the CNT coatings at low pH and in the case of M4_1 coating a higher susceptibility for elevate concentration of chorine ions, present in the saline solution.

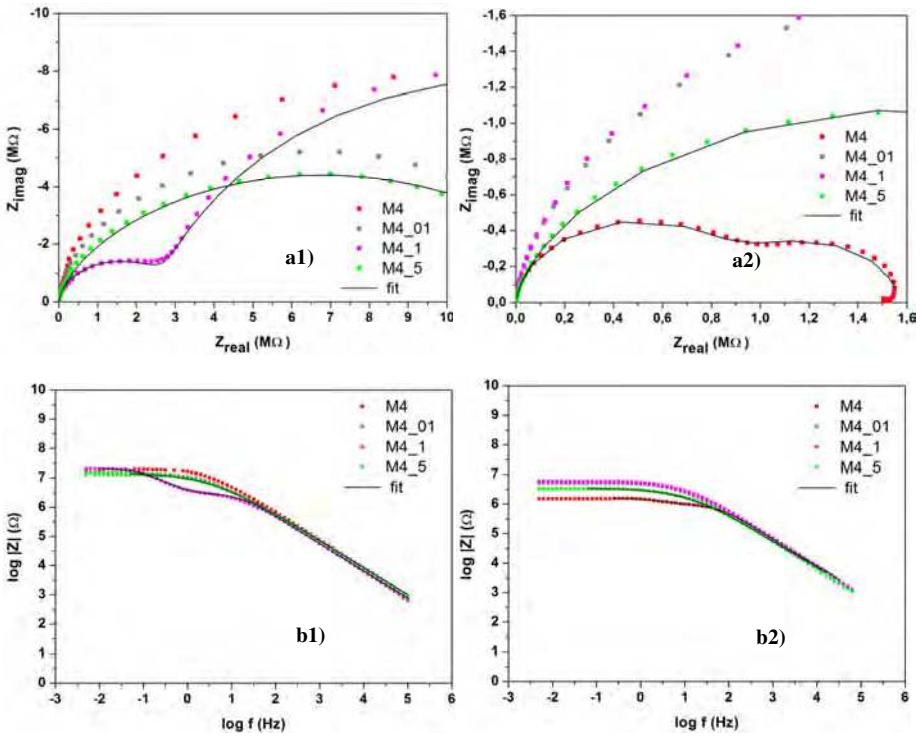

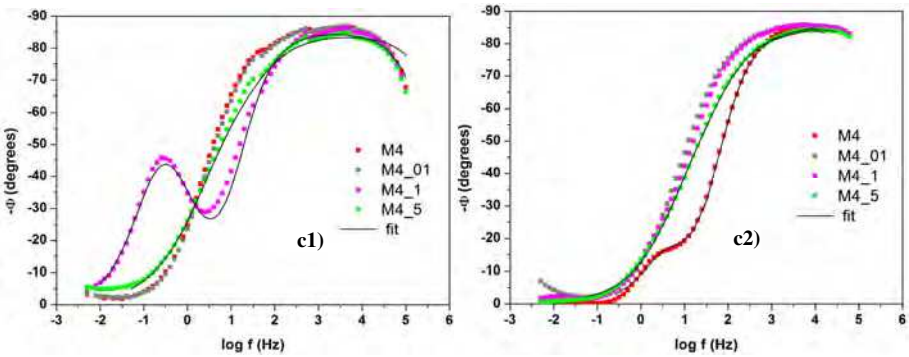

Fig. 15. Complex plane impedance (a), modulus impedance (b) and phase (c) plots of bare carbon steel and hybrids prepared with a MMA/MPTS a ratio of 4 containing CNTs with $[C_{CNT}]/[C_{CNT}+Si]$ molar concentrations of 0% (M4), 0.1% (M4_01), 1.0% (M4_1) and 5% (M4_5) after exposure of 1 day in (1) unstirred and naturally aerated 3.5 % NaCl and (2) 0.05 mol L^{-1} NaCl + 0.05 mol L^{-1} H_2SO_4 solutions. (The small discontinuities of θ vs. log f mark the change of the measurement range of the instrument.)

Sample	M4_5 saline	M4_1 saline	M4_5 acid	M4 acid
χ^2 (10^{-3})	7.2	6.6	0.4	0.9
R_{sol} (Ω cm^2)	27.6 (10.4)*	29.3 (12.2)*	19.5 (8.9)	20.0 (11.2)*
CPE_1 (10^{-3} μF cm^{-2} $s^{\alpha-1}$)	3.95 (3.9)	4.34 (2.4)	39.8 (6.9)	129 (9.9)
n_1	0.93 (0.4)	0.94 (0.3)	0.59 (3.4)	0.89 (4.3)
R_1 (10^6 Ω cm^2)	3.2 (14.9)	2.7 (1.8)	2.51 (0.2)	0.60 (4.7)
CPE_2 (10^{-3} μF cm^{-2} $s^{\alpha-1}$)	18.2 (1.9)	85.2 (1.9)	5.18 (4.9)	3.94 (3.4)
n_2	0.56 (1.5)	0.86 (1.5)	0.93 (0.6)	0.94 (0.4)
R_2 (10^6 Ω cm^2)	1.97 (2.5)	1.63 (2.5)	1.07 (12)	0.94 (1.7)

*Error (%)

Table 3. Parameters of the electrical equivalent circuit for sample M4_5, M4_1 and M4 after 1 day immersion in neutral 3.5% NaCl aqueous and 0.05 mol L^{-1} NaCl + 0.05 mol L^{-1} H_2SO_4 solution.

The higher anti-corrosion efficiency of CNTs containing coatings in acidic medium was confirmed by the comparison of the potentiodynamic polarization curves of the M4 film with those of M4_01, M4_1 and M4_5 coatings, displayed in Figure 16. After 2 h of immersion in acidic NaCl solution the current density of the M4 film is almost one order of magnitude lower than the 10^{-9} Acm^{-2} observed for the CNTs containing coatings (Fig. 16b). Also in the case of exposure to the neutral saline solution (Fig. 16a) the polarization curves of the CNTs samples are very similar showing slightly higher current densities than sample M4, with value of about $8x10^{-10}$ Acm^{-2}. It should be noted, that for all tested films no rupture of the coating was observed in the positive potential branch of the overpotentials of up to 1 V. According to results obtained by scanning electron microscopy and atomic force microscopy the surface of all CNTs containing samples is very smooth with a surface RMS rougness of less than 0.2 nm. Consequently an increase of the anodic current due to larger cathode surface area on increasing doping was not observed. In contrary, Figure 16 shows

that the current density of M4_5 over the anodic potential branch is the lowest in both environments. According to the electrochemical results, the performance against corrosion in neutral saline medium can be established in the following order: M4 > M_5 ≈ M_01 > M_1 > steel. In the case of acidic NaCl solution the established sequence is: M_5 ≈ M_01 ≈ M_1 > M4 > steel. The latter result indicates that the presence of carbon nanotubes in the hybrid structure increases the inert character of the hybrid coatings at low pH values.

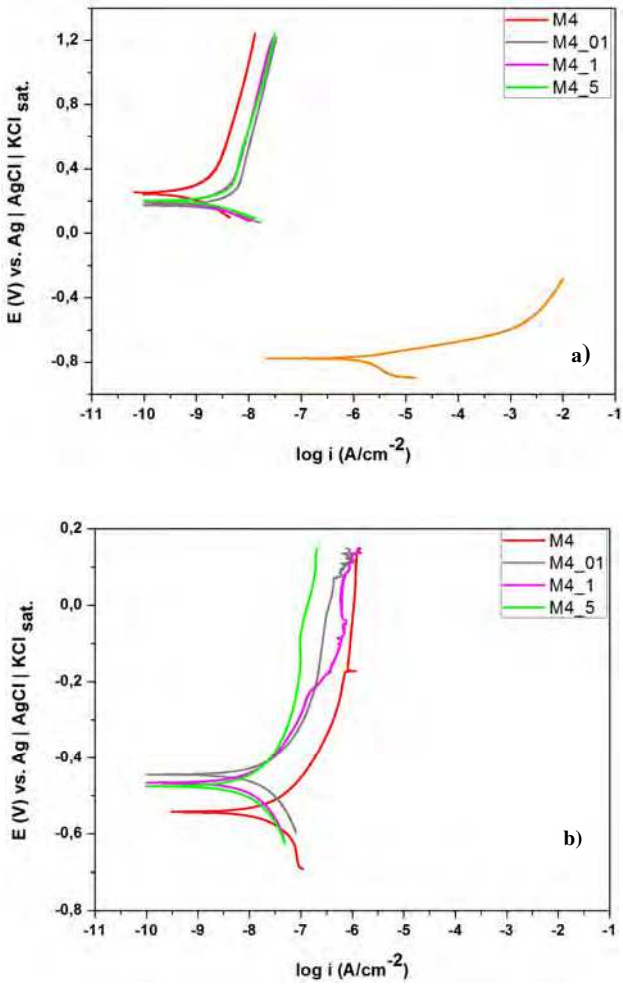

Fig. 16. Potentiodynamic polarization curves of bare carbon steel and hybrids prepared with a MMA/MPTS a ratio of 4 containing CNTs with $[C_{CNT}]/[C_{CNT}+ Si]$ molar concentrations of 0% (M4), 0.1% (M4_01), 1.0% (M4_1) and 5% (M4_5) recorded after 2 h immersion in a) unstirred and naturally aerated 3.5 % NaCl and b) 0.05 mol L^{-1} NaCl + 0.05 mol L^{-1} H_2SO_4 solution.

4. Conclusions

Smooth, crack-free, adherent and optically transparent siloxane-polymethyl methacrylate hybrid coatings were deposited onto carbon steel from sol prepared by acid-catalyzed hydrolytic polycondensation of TEOS and MPTS mixtures at TEOS/MPTS molar ratio of 2, followed by radical polymerization of MMA under varying MMA/MPTS ratio of 2, 4, 8 and 10. XPS results confirmed the increasing proportion of the polymeric phase and NMR results showed that the degree of polycondensation of silicon species had a maximum of about 84% for a MMA/MPTS ratio of 8, while the extent of organic polymerization was essentially unaffected by the variation of MMA. The excellent corrosion protection efficiency of the coatings, with a corrosion resistance of up to 1 GΩ and current density of less than 10^{-10} Acm^{-2} determined by electrochemical measurements for sample M8 is closely related to the ramified structure of siloxane cross-link nodes of the hybrid network. For this sample, no corrosion-induced changes were observed by XPS for up to 18 days of immersion in a NaCl solution. The very high breakdown potential of this coating and the low current density even for high anodic potentials are also indicative for the exceptional performance of these coatings against corrosion. Thus the high polycondensation degree of the inorganic backbone results in the formation of a dense hybrid coating that acts as an efficient diffusion barrier, protecting carbon steel against corrosion, principally in neutral chloride medium.

XPS and TG/DTG results obtained for carbon nanotubes containing hybrids, indicate that the incorporated CNTs increase the stability of the hybrid network possibly by formation of covalent bonds with siloxane groups. Electrochemical measurements have shown similar anti-corrosion characteristics than the undoped samples in neutral saline environment, while a superior performance was detected in acidic NaCl media, due to more inert character of the hybrid structure reinforced by carbon nanotubes.

5. Acknowledgements

The authors like to thank for the financial support for this work provided by CAPES, CNPq and FAPESP.

6. References

Betova, I.; Bojinov, M.; Laitinen, T.; Makela, K.; Pohjanne,P.; Saario, T. (2002). The Transpassive Dissolution Mechanism of Highly Alloyed Stainless Steels: I. Experimental Results and Modeling Procedure. *Corrosion Science*, Vol.44, No.12, (March 2002), pp. 2675 – 2697, ISSN 0010-938X

Bhattacharyya, S.; Das, M.B.; Sarkar. S. (2008). Failure Analysis of Stainless Steel Tubes in a Recuperator Due to Elevated Temperature Sulphur Corrosion. *Engineering Failure Analysis*, Vol.15, No.6, (September 2008), pp. 711 – 722, ISSN 1350-6307

Briggs, D. & M.P. Seah M.P. (1994), *Practical Surface Analysis: Auger and X-ray Photoelectron Spectroscopy*, John Wiley & Sons, ISBN 0-471-92081-9, Chichester, England

Brinker, C. J. & Scherrer, G. W. (1990). *Sol-gel science*, Academic Press, ISBN 13:978-0-12-134970-7, New York

De Graeve, I.; Vereecken, J.; Franquet, A.; Van Schaftinghen, T.; Terryn, H. (2007). Silane Coating of Metal Substrates: Complementary Use of Electrochemical, Optical and

Thermal Analysis for the Evaluation of Film Properties. *Progress in Organic Coating*, Vol.59, No.3, (June 2007), pp. 224 – 229, ISSN 0300-9440

Droppa Jr. R.; Hammer, P.; Carvalho A.C.M.; Dos Santos, M. C.; Alvarez, F. (2001). Incorporation of Nitrogen in Carbon Nanotubes. *Journal of Non-Crystalline Solids,* Vol.299-302, part 2, (April 2002), pp. 874-879, ISSN 0022-3093

Eder. D. (2010). Carbon Nanotube Inorganic Hybrids. *Chemical Reviews*, Vol.110, No.3, (March 2010), pp 1348–1385, ISSN 0009-2665.

Fedrizzi L.; Rodriguez F.J.; Rossi S.; Deflorian F.; Di Maggio R. (2001). The Use of Electrochemical Techniques to Study the Corrosion Behavior of Organic Coatings on Steel pretreated with Sol-Gel Zirconia Films. *Electrochimica Acta*, Vol.46, No.24-25, (August 2001), pp. 3715 – 3724, ISSN 0013-4686

Feliu V.; González J.A.; Andrade C.; Feliu S. (1998). Equivalent circuit for modeling the steel-concrete interface. II. Complications in applying the stern-geary equation to corrosion rate determination. Corros. Sci. Vol.40, No.6, pp. 995-1006, ISSN 0010-938X.

Hammer, P.; Schiavetto, M. G.; dos Santos, F. C.; Pulcinelli, S. H.; Benedetti, A. V.; Santilli, C. V. (2010). Improvement of the Corrosion Resistance of Polysiloxane Hybrid Coatings by Cerium Doping. *Journal of Non-Crystalline Solids,* Vol.356, No. 44-49, (October 2010), pp. 2606 - 2612, ISSN 0022-3093.

Han,Y.H.; Taylor, A.; Mantle, M.D.; Knowles, K.M. (2007). UV curing of organic–inorganic hybrid coating materials. *Journal of Sol–Gel Science and Technology,* Vol.43, No.1, (January 2007), pp. 111 – 123, ISSN 0928-0707

Harreld, J.H.; Esaki, A.; Stucky, G.D. (2003). Low-Shrinkage, High-Hardness, and Transparent Hybrid Coatings: Poly(methyl methacrylate) Cross-Linked with Silsesquioxane. *Chemistry of Materials*, Vol.15, No.18, (July 2003), pp. 3481-3489, ISSN 0897-4756

Innocenzi, P.; Brusatin, G.; Licoccia, S.; Di Vona, M.L.; Babonneau, F.; Alonso, B. (2003). Controlling the Thermal Polymerization Process of Hybrid Organic-Inorganic Films Synthesized from 3-Methacryloxy-propyltrimethoxysilane and 3-Aminopropyltriethoxysilane. *Chemistry of Materials*, Vol.15, No.25, (November 2003), pp.4790 – 4797, ISSN 0897-4756

José, N. M.; Prado, L. A. S. A. (2005). Materiais híbridos orgânico-inorgânicos: preparação e algumas aplicações. *Química Nova*, v.28, No.2, (November 2004), pp. 281-288, ISSN 0100-4042

Khare, R. & Bose, R. (2005). Carbon Nanotubes Based Composits – A Review. *Journal of Minerals & Materials Characterization & Engineering*, Vol.4, No.1, pp. 31-46, ISSN 1539-2511

Kim, M.; Hiong, J.; Hong, C.K.; Shim, S.E. (2009). Preparation of Silica-Layered Multi-Walled Carbon Nanotubes Activated by Grafting of Poly(4-vinylpyridine). *Synthetic Metals,* Vol.159, No.1-2, (January 2009), pp. 62-68, ISSN 0379-6779

Landry, C. J. T.; Coltrain, B.K.; Brady, B.K. (1992). In Situ Polymerization of Tetraethoxysilane in poli(methyl methacrylate): Morphology and Dynamic Mechanical Properties. *Polymer*, Vol.33, No.7, (February 1991), pp. 1486 – 1494, ISSN 0032-3861

Lopez, D.A; Rosero-Navarro, N.C.; Ballarre, J.; Durán, A.; Aparicio, M.; Ceré, S. (2008). Multilayer Silica-methacrylate Hybrid Coatings Prepared by Sol–Gel on Stainless

Steel 316L: Electrochemical Evaluation. *Surface & Coatings Technology*, Vol.202, No.10, (February 2008), pp. 2194 – 2201, ISSN 0257-8972

Masalski, J.; Gluszek, J.; Zabrzeski, J.; Nitsch, K.; Gluszek, P. (1999). Improvement in Corrosion Resistance of the 3161 Stainless Steel by Means of Al_2O_3 Coatings Deposited by Sol-Gel Method. *Thin Solid Films*, Vol.349, No.1, (July 1999), pp. 349 186 – 190, ISSN 0040-6090

Messaddeq, S. H.; Pulcinelli, S. H.; Santilli, C. V.; Guastaldi, A. C.; Messaddeq, Y. (1999). Microstructure and Corrosion Resistance of Inorganic-Organic (ZrO_2-PMMA) Hybrid Coating on Stainless Steel. *Journal of Non-Crystalline Solids*, Vol.247, No.2, (December 1999), pp. 164-170, ISSN 0022-3093

Metroke, T. L.; Kachurina, O.; Knobbe, E. T. (2002). Spectroscopic and Corrosion Resistance Characterization of GLYMO-TEOS Ormosil Coatings for Aluminum Alloy Corrosion Inhibition. *Progress in Organic Coatings*, Vol.44, No.4, (August 2002), pp. 295-305, ISSN 0300-9440

Nazeri, A; TrzaskomaPaulette, P.P.; Bauer, D. (1997). Synthesis and Properties of Cerium and Titanium Oxide Thin Coatings for Corrosion Protection of 304 Stainless Steel. *Journal of Sol–Gel Science and Technolology*, Vol.10, No.3, (November 1997), pp. 317 – 331, ISSN 0928-0707

Pepe, A.; Aparicio, M.; Cere, S.; Duran, A. (2004). Preparation and Characterization of Cerium Doped Silica Sol-Gel Coatings on Glass and Aluminum Substrates. *Journal of Non-Crystalline Solids,* Vol.348, No.15, (November 2004), pp. 162-171, ISSN 0022-3093

Ryan, M.R.; Williams, D.E. ; Chater, R.J.; Hutton, B.M ; McPhail, D.S. Why Stainless Steel Corrodes. (2002). *Nature,* Vol.415, No.6873, (February 2002), pp. 770- 774, ISSN 0028-0836

Sanchez, C. & Lebeau, B. (2004). Optical Properties of Functional Hybrid Organic-Inorganic Nanocomposites, In: *Functional Hybrid Material*, Gómez-Romero, P., pp. (122-168), Oxford: Elsevier, ISBN 3-527-30484-3, Germany

Saravanamuttu, K.; Du, X. M.; Najafi, S.I.; Andrews, M.P. (1998). Photo-induced Structural Relaxation and Densification in Sol-Gel Derived Nanocomposite Thin Films; Implications in Integrated Optics Device Fabrication. *Canadian Journal of Chemistry / Revue Canadienne de Chimie*, Vol.76, No.11, (November 1998), pp.1717 – 1729, ISSN 1480-3291

Sarmento, V. H. V.; Frigerio, M.R.; Dahmouche, K.; Pulcinelli, S. H.; Santilli, C. V. (2006). Evolution of Rheological Properties and Local Structure During Gelation of Siloxane-Polymethylmethacrylate Hybrid Materials. *Journal of Sol–Gel Science and Technology*, Vol.37, No.3, (February 2006), pp. 179 – 174, ISSN 0928-0707

Sarmento, V.H.V.; Schiavetto, M.G.; Hammer, P.; Benedetti, A.V.; Fugivara, C.S.; Suegama, P.H.; Pulcinelli, S.H.; Santilli, C.V. (2010). Corrosion Protection of Stainless Steel by Polysiloxane Hybrid Coatings Prepared Using the Sol-Gel Process. *Surface & Coatings Technology*, Vol.204, No.16-17, (February 2010), pp. 2689-2701, ISSN 0257-8972

Stern, M.; Geary A.L. (1957). Electrochemical polarization. Journal of Electrochem. Soc., Vol.104, No.1, pp. 56-63, ISSN 1945-7111.

Suegama, P.H.; de Melo, H.G.; Benedtti, A. V.; Aoki, I.V. (2009). Influence of Cerium (IV) Ions on the Mechanism of Organosilane Polymerization and on the Improvement of its Barrier Properties. *Electrochimica Acta,* Vol.54, No.9, (March 2009), pp. 2655-2662, ISSN 0013-4686

Suegama, P.H.; Espallargas, N.; Guilemany, J. M.; Fernández, J.; Benedetti, A. V. (2006). Electrochemical and Structural Characterization of Treated Cr_3C_2-NiCr Coatings. *Journal of Electrochemical Society,* Vol.153, No.10, pp. B434-B445, ISSN 1945-7111

Tadanaga K. ; Ellis B. ; Seddon A.B. (2000). Near- and Mid-Infrared Spectroscopy of Sol-Gel Derived Ormosil Films for Photonics from Tetramethoxysilane and Trimethoxysilylpropylmethacrylate. *Journal of Sol–Gel Science and Technology,* Vol.19, No.1 – 3, (December 2000), pp. 687 - 690, ISSN 0928-0707

Tsutsumi, Y.; Nishikata, A.; Tsuru, T. (2007). Pitting corrosion mechanism of Type 304 stainless steel under a droplet of chloride solutions. *Corrosion Science*, Vol. 49, No.3, (October 2006), pp. 1394 – 1407, ISSN 0010-938X

Vasconcelos, D.C.L.; Carvalho, J.A.N.; Mantel, M.; Vasconcelos, W.L. (2000). Corrosion Resistance of Stainless Steel coated with Sol-Gel Silica. *Journal of Non–Crystalline Solids*, Vol.273, No.1-3, (August 2000), pp. 135 – 139, ISSN 0022-3093

Voiry, D.; Vallés, C.; Roubeau, O.; Pénicaud, A. (2011). Dissolution and alkylation of Industrially Produced Multi-Walled Carbon Nanotubes. *Carbon,* Vol.49, No.1, (January, 2011), pp. 170-175, ISSN 0008-6223.

Wang, Y. & Bierwagen, G.P.P. (2009). A New Acceleration Factor for the Testing of Corrosion Protective Coatings: Flow-Induced Coating Degradation. *Journal of Coatings Technology and Research*, Vol.6, No.4, (December 2009), pp. 429-436, ISSN 1547-0091

Zandi-Zand, R.; Ershad-Langroudi, A.; Rahimi, A. (2005). Organic-Inorganic Hybrid Coatings for Corrosion Protection of 1050 Aluminum Alloy. *Journal of Non-Crystalline Solids*, Vol.351, No.14-15, (May 2005), pp. 1307-1311, ISSN 0022-3093

Zheng, S. & Li, J. (2010). Inorganic–Organic Sol Gel Hybrid Coatings for Corrosion Protection of Metals. *Journal of Sol-Gel Science and Technology*, Vol.54, No.2, (May 2010), p. 174-187, ISSN 0928-0707

Zheludkevich, M.L.; Salvado, I.M.; Ferreira, M.G.S. (2005). Sol-gel Coatings for Corrosion Protection of Metals. Journal of Materials Chemistry, Vol.15, No.18, (July 2005), pp. 5099-5111, ISSN 0959-9428

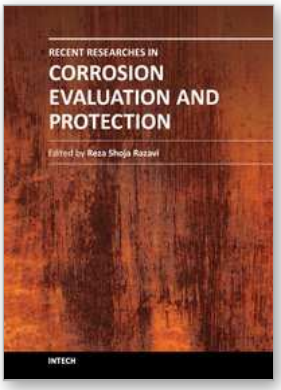

Recent Researches in Corrosion Evaluation and Protection

Edited by Prof. Reza Shoja Razavi

ISBN 978-953-307-920-2
Hard cover, 152 pages
Publisher InTech
Published online 25, January, 2012
Published in print edition January, 2012

The purpose of this book is to present and discuss the recent methods in corrosion evaluation and protection. The book contains six chapters. The aim of Chapter 1 is to demonstrate that Electrochemical Impedance Spectroscopy can be a very useful tool to provide a complete evaluation of the corrosion protection properties of electro-coatings. Chapter 2 presents results of studies of materials degradation from experimental electrochemical tests and theoretical calculations. Chapter 3 deals with the presentation of the corrosion and corrosion prevention of the aluminum alloys by organic coatings and inhibitors. Chapter 4 addresses the new method of pigment preparation that can improve protection efficiency. The effectiveness of plasma deposited films on the improvement of carbon steel corrosion resistance is discussed in Chapter 5. Chapter 6 deals with the conjugation of carbon nanotubes with organic-inorganic hybrid to prepare hybrid coatings that combine high anti-corrosion efficiency with elevated mechanical resistance.

INTECH
open science | open minds

InTech Europe
University Campus STeP Ri
Slavka Krautzeka 83/A
51000 Rijeka, Croatia
Phone: +385 (51) 770 447
Fax: +385 (51) 686 166
www.intechopen.com

InTech China
Unit 405, Office Block, Hotel Equatorial Shanghai
No.65, Yan An Road (West), Shanghai, 200040, China
中国上海市延安西路65号上海国际贵都大饭店办公楼405单元
Phone: +86-21-62489820
Fax: +86-21-62489821